Journal of Renewable Materials

Tech Science Press

DOI: 10.32604/jrm.2024.049810

ARTICLE

One-Step to Prepare Lignin Based Fluorescent Nanoparticles with Excellent Radical Scavenging Activity

Xujing Zhang[1], Hatem Abushammala[2], Debora Puglia[3], Binbao Lu[1], Pengwu Xu[1], Weijun Yang[1,*] and Piming Ma[1]

[1]The Key Laboratory of Synthetic and Biological Colloids, Ministry of Education, School of Chemical and Material Engineering, Jiangnan University, Wuxi, 214122, China

[2]Environmental Health and Safety Program, College of Health Sciences, Abu Dhabi University, P.O. Box 59911, Abu Dhabi, United Arab Emirates

[3]Civil and Environmental Engineering Department, Materials Engineering Center, Perugia University, UdR INSTM, Terni, 05100, Italy

[*]Corresponding Author: Weijun Yang. Email: weijun.yang@jiangnan.edu.cn

Received: 18 January 2024 Accepted: 06 March 2024 Published: 17 July 2024

ABSTRACT

Fluorescent nanomaterials have attracted much attention, due to their unique luminescent properties and promising applications in biomedical areas. In this study, lignin based fluorescent nanoparticles (LFNP) with high yield (up to 32.4%) were prepared from lignin nanoparticles (LNP) by one-pot hydrothermal method with ethylenediamine (EDA) and citric acid. Morphology and chemical structure of LFNP were investigated by SEM, FT-IR, and zeta potential, and it was found that the structure of LFNP changed with the increase of citric acid addition. LFNP showed the highest fluorescence intensity under UV excitation at wavelengths of 375–385 nm, with emission wavelengths between 454–465 nm, and exhibited strong photoluminescence behavior. Meanwhile, with the increase of citric acid content, the energy gap (ΔE) gradually decreased from 3.87 to 3.14 eV, which corresponds to the gradual enhancement of fluorescence performance. LFNP also exhibited excellent antioxidant activity, with DPPH free radical scavenging rate increased from 80.8% for LNP up to 96.7% for LFNP, confirming the great potential of these materials for application in biomedicine and cosmetic health care.

KEYWORDS

Lignin; fluorescent nanoparticles; bioactivity; photoluminescence mechanism

1 Introduction

Lignin is a naturally occurring three-dimensional amorphous polymer with a unique aromatic ring structure, composed of p-hydroxyphenyl (H), guaiacyl (G), and syringyl (S) linked by C-C and C-O bonds [1–4]. Lignin is mainly from wastewater from the pulp and paper industry, also known as papermaking black liquor, which is usually discharged into rivers or used as a low-value fuel to provide heat and electricity generation, resulting in considerable waste of this resource and environmental pollution. Various types of lignin with different amounts of monomers and bonds can be produced from different sources and pulping processes, such as milled wood lignin (MWL) [5], alkali lignin (AL), Kraft lignin (KL), and enzymatic lignin [6,7].

Fluorescent nanomaterials are mainly composed of small amounts of molecules or atoms of carbon, hydrogen, oxygen and other elements with good fluorescence properties. Compared to conventional semiconductor quantum dots, new fluorescent nanomaterials not only need to be chemically resistant, environmentally friendly, having long-range stable luminescence, tunable photoluminescence behavior, and easy to be chemically modified, but also need to be well dispersed in water, biocompatible, and biologically non-toxic. The materials can be applied in emerging fields, such as ionic detection [8], biomedicine, energy storage, display devices, and catalysis [9–11]. Both "top-down" and "bottom-up" approaches are often used to synthesize fluorescent nanoparticles [12,13]. Top-down methods include laser ablation, arc discharge and electrochemical oxidation, in which nanoparticles are generated or "fractured" from larger carbon materials [11]. Bottom-up methods involve obtaining fluorescent nanoparticles from small-molecule organic precursors, including plasma methods, ultrasonic methods, and hydrothermal treatment methods [14–16].

However, many of these synthetic methods involve the use of costly or toxic raw materials, long reaction times, high temperatures, and surface-passivation [17]. Also, high cost of raw materials and low yields hinder industrial applications. Recently, various biomass feedstocks (bananas, fruit juices, cherries, rice hulls, etc.) have been used as carbon precursors to address these issues [18,19]. So far, many researchers have reported different value-added methods for modifying lignin and synthesizing lignin-based polymers, such as phenolic resins [20,21], epoxy polymers, polyurethanes [22–24], and carbon fibers [25].

Currently, the relevant properties of lignin fluorescent nanomaterials have received extensive attention [26]. Chen et al. synthesized fluorescent nanomaterials for the first time by hydrothermal method by modifying lignin with hydrogen peroxide as an oxidizing agent, but the bioactive efficiency, quantum yield, and kind of lignin precursor used were not referred [27]. Ding et al. reported the gram scale synthesis of single crystal GQDs derived from lignin biomass using a two-step method of oxidative cracking and aromatic reduction using alkaline lignin molecules, but there are problems with long reaction time and high energy waste [28]. Liang et al. prepared fluorescent nanomaterials rich in surface amines using xylan as a carbon source, ammonia solution as a solvent, and passivation agent through hydrothermal method [29]. The quantum yield was improved after passivation modification. In addition, Liang et al. found that compared to commonly used amine end capping passivators such as ethylenediamine, ammonia can form more stable surface defects, thereby inducing stronger fluorescence emission. The degree of surface passivation also had a significant impact on the luminescence stability. Xie et al. modified lignin with different additions of ethylenediamine using highland barley as a carbon source [30]. They found that the quantum yield increased from 6.2% to 14.4% and the fluorescence performance remained stable. Pang et al. synthesized N-doped fluorescent nanomaterials from alkali lignin and diethylenetriamine (DETA) by a one-pot solvothermal method [31], it was found that the nanomaterials had better sensitivity and selectivity for Co^{2+} and Fe^{3+} ions as fluorescent nanosensors. Although these studies mentioned above can effectively improve the fluorescence performance of lignin, they are mainly based on lignin-fluorescent carbon quantum dots, which generally have low yields and small particle sizes, are not easy to collect, and neglect the exploration of lignin's own bioactivity.

This paper presents a simple one-step hydrothermal method to synthesize lignin based fluorescent nanoparticles (LFNP) via the interaction of lignin, citric acid (CA), and ethylenediamine (EDA). We prepared nitrogen-doped modified lignin by doping nitrogen elements and biomass raw materials through hydrothermal reaction. And the effect of citric acid addition on the performance of modified lignin was explored, and attention was paid to the yield, particle size, and antioxidant activity of the prepared lignin. These induced amination reactions introduce hydrophilic amines and amide groups into the lignin structure, which possesses higher yields and larger particle sizes compared to lignin-based carbon quantum dots. The influence of different amounts of CA and EDA addition on the performance and morphology of LFNP was also discussed. Scanning electron microscopy (SEM), Fourier transform

infrared spectroscopy (FT-IR), zeta potential and fluorescence spectroscopy are used to characterize LFNP, and the antioxidant activity of LFNP is investigated by using DPPH radical scavenging method.

2 Materials and Methods

2.1 Materials

Enzymatic lignin (Lignin, provided by Shandong Longli Bio-technology Co., Ltd., China), citric acid (CA) was purchased from Sinopharm Chemical Reagent Company (Shanghai, China) without further treatment, ethylenediamine (EDA) was purchased from Macklin to realize a 75% ethylenediamine solution. 1,1-Diphenyl-2-picrylhydrazyl radical 2,2-Diphenyl-1-(2,4,6-trinitrophenyl) hydrazyl (DPPH) was purchased from Macklin. The other required materials or solvents were purchased from Sinopharm Chemical Reagent Company.

2.2 Preparation of Lignin Based Fluorescent Nanoparticles (LFNP)

Lignin nanoparticles (LNP) were prepared in accordance with previously available methods [32]. Lignin based fluorescent nanoparticles were prepared by a simple one-pot hydrothermal method by varying the ratios of different LNP, CA and EDA according to the formulations listed in Table 1, and the products were named as LFNP-1, LFNP-2 and LFNP-3, respectively. The specific experimental steps were as follows: lignin was dispersed in water of deionized water by stirring for 15 min, and then EDA was added. Added citric acid after the solution cools to room temperature. Finally, poured the mixed solution into a hydrothermal reactor for reaction at 180°C for 4 h. The products were purified by centrifugation for 30 min and dialyzed using a dialysis bag with a molecular weight of 3500 Da for 3 days: the resultant yellow solutions were obtained, and the yield of LFNP-1, LFNP-2 and LFNP-3 were found to be equal to 24.0%, 24.8% and 26.1%, respectively (Fig. 1).

Table 1: Formulations of the LFNP

Samples	LNP	EDA (75%)	CA
LFNP-1	0.1 g	4.625 g	1.92 g
LFNP-2	0.1 g	4.625 g	3.84 g
LFNP-3	0.1 g	4.625 g	5.76 g

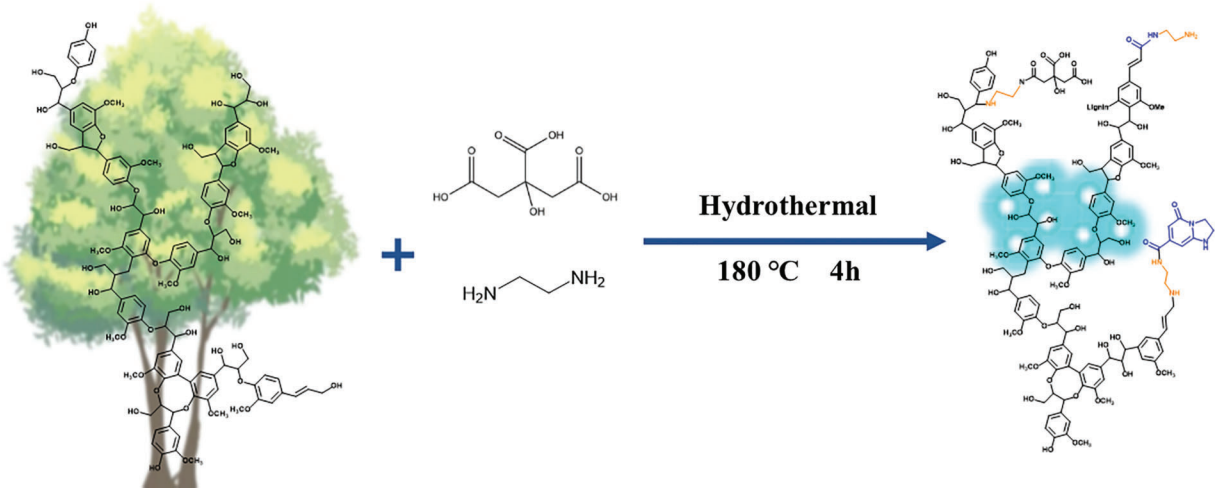

Figure 1: Process of modifying lignin with different amounts of citric acid and ethylenediamine

2.3 Characterizations

The infrared spectroscopic characteristics of LNP and LFNP were assessed throughout FT-IR (Nicolet iS50, Thermo Fisher Scientific, USA), by using a spectral width of 4000~800 cm^{-1} and 32 scans per sample. Zeta potential experiments were performed using a Zeta Potential and Nanoparticle Analyzer (Zeta PALS, Bruker, USA). The sample solution concentration was 1 mg/mL and all experiments were performed at room temperature. Each sample was measured three times and the average value was obtained.

Photoluminescence measurements using the Varian CARY Eclipse fluorescence spectrophotometer. The fluorescence test parameter is a scanning speed of 200 nm/min; slit width 5.0 nm; The response time is 0.5 s, and the reproducibility is ±0.2 nm. Equipped with a xenon lamp as the excitation source. The solvent used for fluorescence testing was water with a concentration of 0.1 g/mL. The solution was treated by ultrasonic dispersion before the measurements.

Antioxidant activity was evaluated in the range of 200-800 nm by using a UV spectrophotometer [33,34]. Radical scavenging activity (RSA) was measured by DPPH assay. DPPH solution (50 mg/L, 2 mL) and sample solution (1 mg/mL, 2 mL) were mixed and left in the dark for 1 h to ensure complete reaction, with the ethanol replacing the sample as a control. Subsequently, the absorbance at 517 nm of the blank control and samples was tested using a dual-beam UV-visible spectrophotometer (TU-1950, Presee, China) with a medium scanning speed, a scanning range of 200–800 nm and three scans for each sample.

The absorbance curves in the wavelength range of 500–530 nm were area fitted to calculate the area S. The RSA can be calculated according to the following equation:

$$\mathrm{RSA} = \frac{S_{control} - S_{sample}}{S_{control}} \times 100\% \quad (1)$$

$S_{control}$ and S_{sample} denoted the fitted area of the absorbance curves in the wavelength range of 500–530 nm for the blank control and the sample solution, respectively.

3 Results and Discussion

3.1 Morphology and Structure

Fig. 2 shows a comparison of SEM images of LNP and LFNP. SEM characterization of the LFNP sample revealed that the unmodified LNP exhibit aggregated and random shapes. In addition, the nanoparticles treated with citric acid and ethylenediamine gradually showed a more regular shape with a smoother surface, and the particle size gradually increased with the addition of citric acid. The comparison of LFNP samples prepared with different raw material ratios showed that the sizes of LFNP-1 and LFNP-2 still had smaller particle sizes dispersed, while the nanoparticle sizes of LFNP-3 were uniformly distributed in the range of 250–350 nm, with the most regular morphology. These results proved that the reaction between lignin and citric acid resulted to changes in the surface morphology and internal structure of the original lignin nanoparticles, thus manifesting the increase to larger diameter spherical nanoparticles, and this phenomenon was also related to a cross-linking reaction [35].

Zeta potential can corroborate the change in morphology of LFNP samples. As shown in Fig. 3, the Zeta potential of LNP was −24.5 mV, and the Zeta potential of LFNP tended to increase with the addition of citric acid. −OH is the main reason for the negative charge of lignin, and oxidation to carboxyl groups or acylation with citric acid and ethylenediamine leads to a decrease in negative charge, so a decrease in the absolute value of the Zeta potential could also be evidence for the synthesis of LFNP.

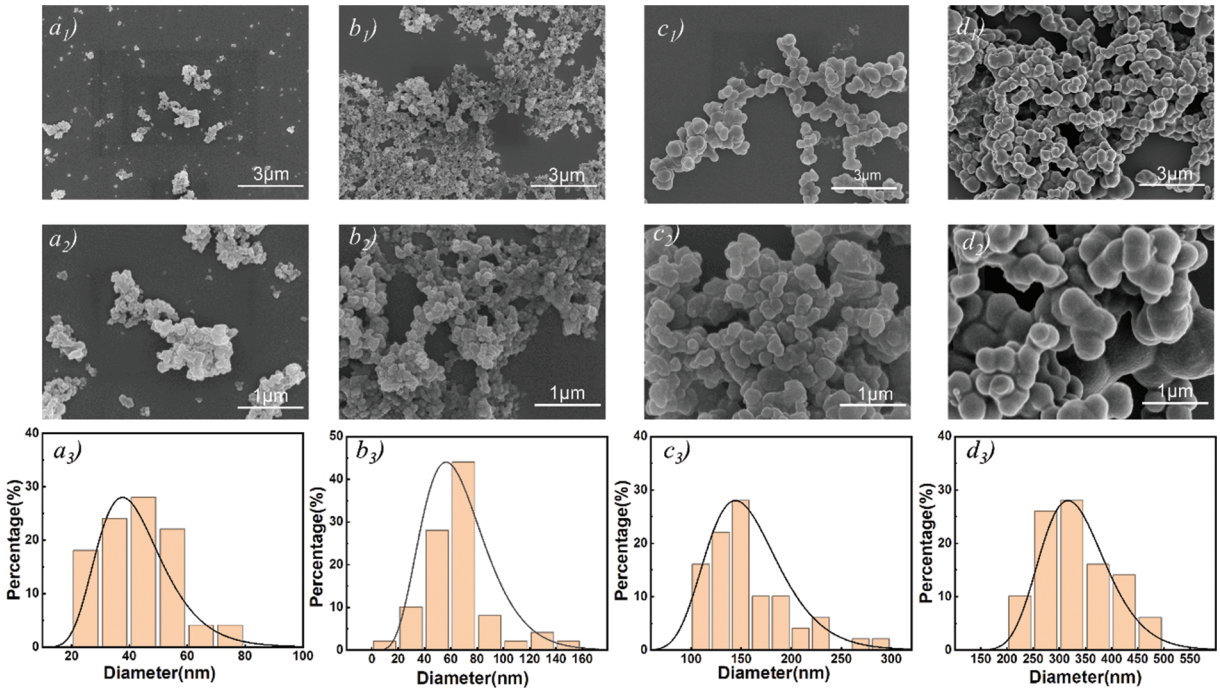

Figure 2: SEM images and particle size distribution of modified lignin, (a_1–a_3) LNP; (b_1–b_3) LFNP-1; (c_1–c_3) LFNP-2; (d_1–d_3) LFNP-3

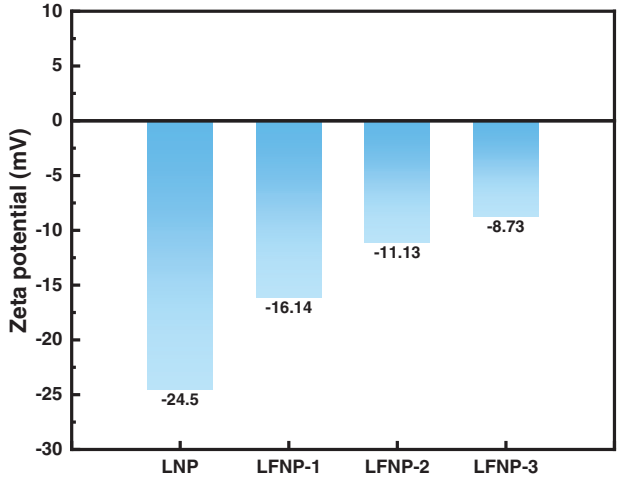

Figure 3: The zeta potential of LNP and LFNP

The LFNP samples were further characterized for their chemical structures [36,37]. Fig. 4 shows the FTIR spectra of 4000~600 cm^{-1}, as well as magnified regions that are particularly sensitive to structural changes between 1500 and 1800 cm^{-1}. As shown in Fig. 4a, the broad peak at 3398 cm^{-1} was attributed to the stretching vibration of the O-H moiety, and the peak at 2945 cm^{-1} was attributed to the C-H stretching of the methyl or methylene group. The four peaks at 1593, 1511, 1462, and 1424 cm^{-1} were

associated to the aromatic skeleton of lignin, with the characteristic absorptions of LNP [38,39]. Characteristic peaks of lignin at 1593 cm^{-1} were also present in sample LFNP compared to LNP. The peak located at 1651 cm^{-1} showed a vibration belonging to -CO-NH-, which proved that acylation reactions between certain polar groups occurred during the process [40,41]. By comparison, it was observed that the out of plane bending vibration of C-H increased at 820 cm^{-1}, confirming that amine grafting caused a change in strength. Semi-quantitative analysis of the infrared maps in the range of 1630–1680 cm^{-1} was carried out to calculate the integral area, which increased from 2.755 for LFNP-1 to 5.478 for LFNP-3 as shown in Fig. 4b, amide-bonded moieties and luminescent cluster structures provide proof of the later fluorescent and antioxidant performance enhancement.

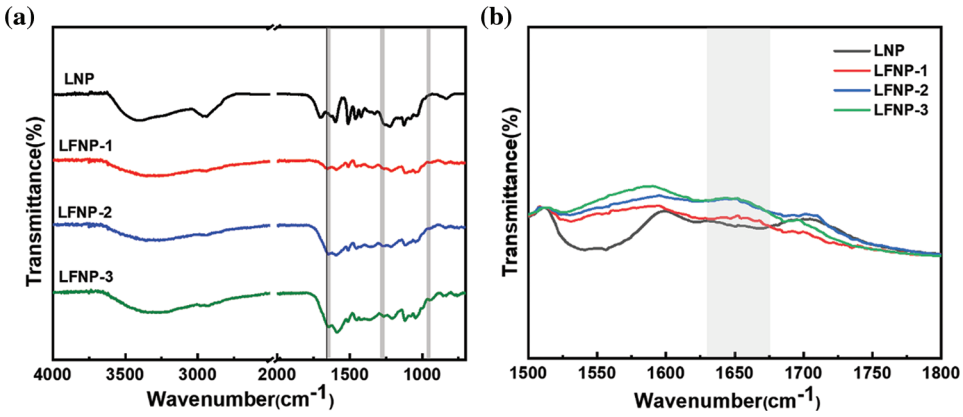

Figure 4: (a) The FT-IR spectra of LNP, LFNP-1, LFNP-2 and LFNP-3; (b) Enlarged view of 1500–1800 cm^{-1} range

3.2 Fluorescence Properties

The excitation and emission spectra of LFNP were shown in Fig. 5. When the excitation wavelength was 380 nm, the emission intensity of all three LFNP reached the maximum, the maximum emission peak of LFNP-1 was located at 454 nm, the maximum emission peak of LFNP-2 was located at 455 nm, and that of LFNP-3 was located at 465 nm, with a maximum fluorescence intensity. These different fluorescence intensities could be attributed to the fact that, with the increase in citric acid content in the LFNP, the sp^2 and sp^3 hybridization in LFNP with increasing citric acid content was obtained [10,42]. It was also found that under UV irradiation, the prepared LFNP had high fluorescence stability at longer irradiation times.

The energy gap (ΔE) is an important parameter of photoluminescent materials, which refers to the energy difference between the highest occupied molecular orbital (HOMO) and the lowest unoccupied molecular orbital (LUMO) in the material [43–45]. Therefore, the energy gap determines whether the photoluminescent material can be excited by a specific wavelength of light and what color luminescence is produced. It can be considered that fluorescence is one of the manifestations of a molecule's transition between the ground and excited states after absorbing energy.

The common methods used to calculate the energy gap are spectroscopic testing and conductivity testing. The common methods used to calculate the energy gap are spectroscopic testing and conductivity testing. The optical gap of LFNP is obtained by measuring the absorption spectrum of the sample using a UV-Vis spectrophotometer Eq. (2).

$$(\alpha hv)^2 = B(hv - \Delta E) \tag{2}$$

where α is the absorbance, hv is the photon energy, h is Planck constant ($h \approx 4.136 \times 10^{-15}$ eV·s), and v is the incident photon frequency ($v = \frac{c}{\lambda}$), where c is the speed of light, λ is the wavelength of the incident light, B is the proportionality constant, and ΔE is the energy gap of the material.

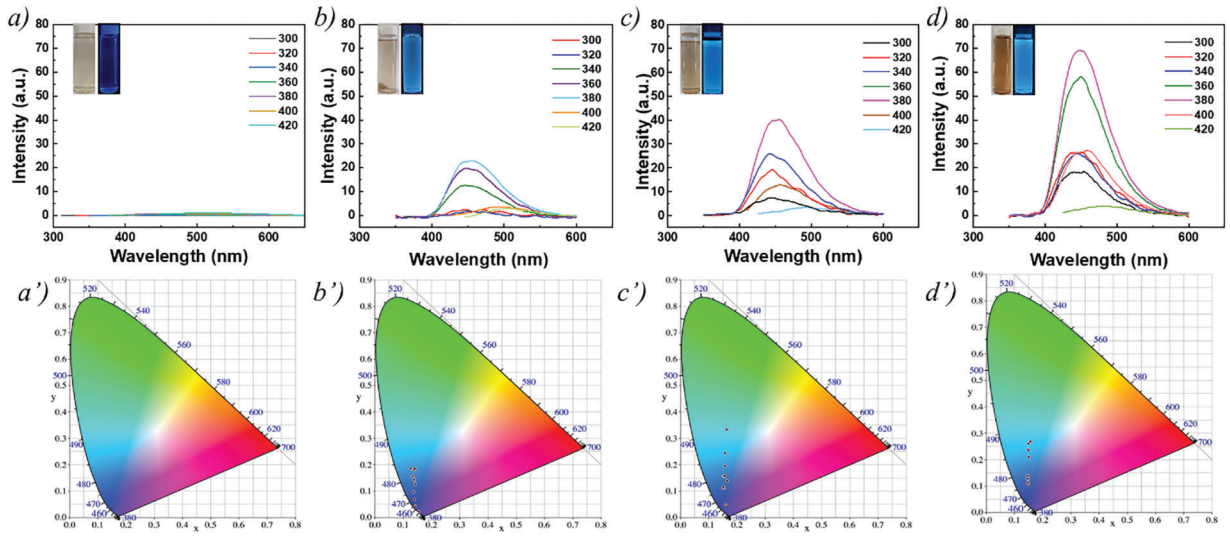

Figure 5: Fluorescence and CIE spectra of citric acid modified lignin with different qualities (a, a') LNP; (b, b') LFNP-1; (c, c') LFNP-2; and (d, d') LFNP-3

The optical properties of LNP and LFNP were investigated by UV-Vis spectrophotometer [31,46]. As shown in Fig. 6, due to the structure of LNP, its UV-vis absorption spectrum had a clear absorption band at 280–290 nm, and the results may be attributed to the typical absorption of aromatic π-systems and the n–π* leaps of carbonyls and other oxygen-containing groups [33,47]. The included figure is a schematic diagram of energy level transitions. The UV jumps of the LFNP modified by citric acid and ethylenediamine were shown in Figs. 6a–6d and the optical band gap was calculated by combining Eq. (2) [48]. A simplified variation of Eq. (2) yields $(\alpha hv)^2$ *vs.* hv, where $hv = \frac{hc}{\lambda} \approx \frac{1240}{\lambda}$. The converted curve was shown as a'–d' in Fig. 6, the image was roughly a turn first, and then there was a section of nearly straight line. We need to intercept this section of the approximate straight-line part of the linear fit, the linear equation in the x-axis intercept was the value of the desired forbidden bandwidth. The energy gap ΔE of the sample can be obtained from a'–d' in Fig. 6. It can be seen that the fluorescence spectra and fluorescence properties of the three samples were very different. In order to find the reason for this phenomenon, the fluorescence mechanism of the three samples of LFNP was explored. As shown in the accompanying figure in Fig. 6, it can be found that the ΔE between the Lowest Unoccupied Molecular Orbital (LUMO) and Highest Occupied Molecular Orbital (HOMO) orbitals of LNP, LFNP-1, LFNP-2, and LFNP-3 were 3.87, 3.70, 3.56, and 3.14 eV, respectively, with the gradual increase of the citric acid addition and a gradual decrease of ΔE. This corroborated with the previous fluorescent properties [49–53].

In fact, some articles had reported on the photoluminescence behavior of lignin in different solvents, such as DMSO, ethanol, THF, chloroform, or γ-valerolactone, it was found that solvents also have a certain influence on the fluorescence behavior of lignin [54–56]. Due to the addition of ethylenediamine and citric acid, some structural changes occurred. This is the primary factor should be taken into consideration. nitrogen-containing groups enhance the luminescence behavior of various materials by forming conjugated structures, meanwhile the abundant electron rich atoms and structures in lignin form luminescent clusters. Both effectively promote the photoluminescence behavior of lignin.

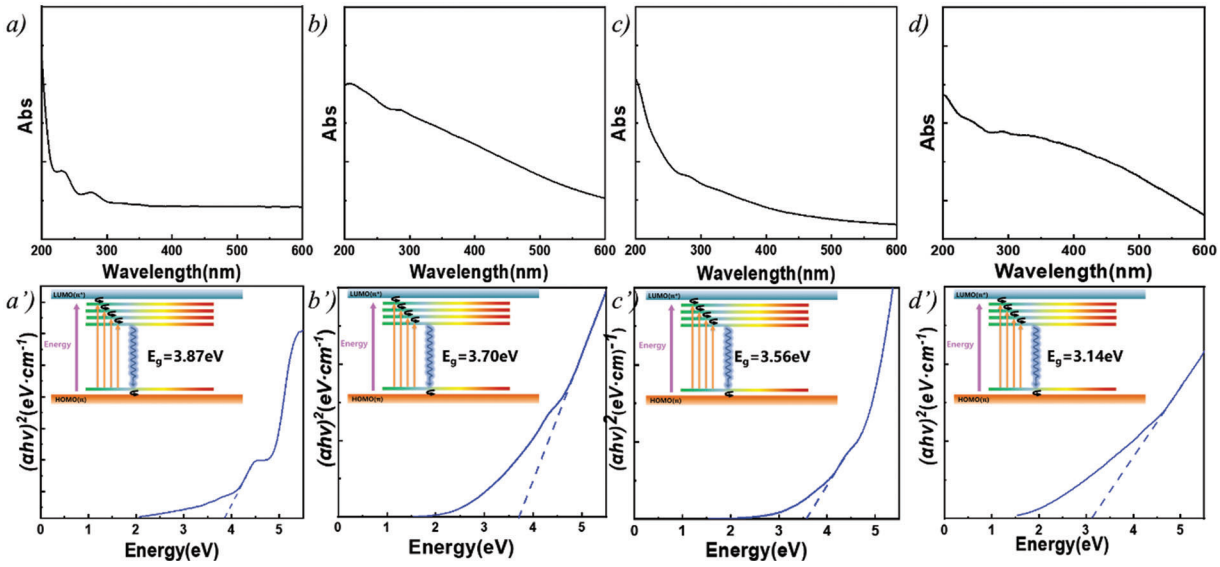

Figure 6: UV Spectra and Transitions of different particles, (a, a') LNP; (b, b') LFNP-1; (c, c') LFNP-2; and (d, d') LFNP-3

It can be hypothesized that the charge transfer between the amine and amide groups and the benzene ring suggests the presence of a donor-acceptor structure and the formation of luminescent clusters through spatial interactions promotes luminescence, which is consistent with previous speculations. In the LFNP, the electron cloud was mainly distributed on the nitrogen-containing groups, whereas in the unmodified nano-lignin, the electron cloud and was mainly distributed on the benzene ring and hydroxyl group. As shown in Fig. 7, the high electron density and nucleophilicity of the modified nitrogen-containing groups induced charge transfer, which implied that the nucleophilic amine attacked the C-O and formed the amide group, thereby inducing formation of the amide group. This can be confirmed by calculating the semi quantitative analysis of -CO-NH- in the FT-IR. and the amine groups directly attached to the benzene ring enhanced the conjugation, and the electron cloud was mainly distributed on the amine groups, amide groups, and cyclic luminescent clusters, leading to a decrease in band gap energy. This also proves that the introduction of amine groups is a key factor to improve the photoluminescence performance. The grafting of amide groups and luminescent clusters onto the lignin benzene ring brings the atoms closer to each other, thus facilitating intramolecular charge transfer, which is enhanced by bonding and/or spatial interactions [57–61]. Luminescent clusters promote luminescence through the formation of spatial interactions. Nitrogen-containing groups and carboxyl groups on citric acid effectively shorten the distance between atoms and are improved by spatial interactions in LFNP, resulting in more stable structures. With the increase of citric acid addition, the content of amide structures and luminescent cluster structures increased, effectively promoting luminescence of lignin. In the FT-IR peak analysis, vibrations belonging to -CO-NH- indicate the presence of acylation reactions between functional groups. At the same time, through semi-quantitative analysis, both the changes in group strength caused by the participation of EDA and CA in the reaction and the increase in calculated integral area are important reasons for the performance changes. It is worth mentioning that due to the presence of two primary amine groups in EDA, it may also undergo various subsequent reactions (namely the bifunctional groups of EDA).

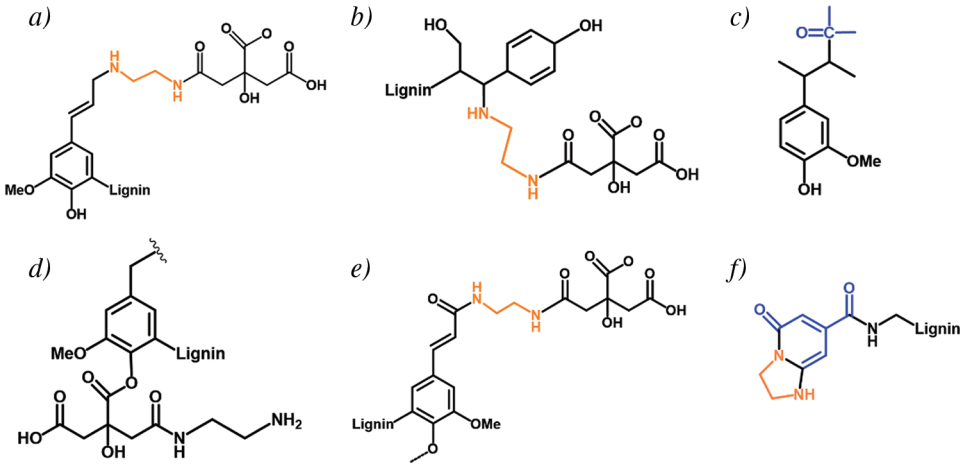

Figure 7: Possible reaction of LFNP synthesized by lignin, CA and EDA

3.3 Antioxidant Properties

The antioxidant properties of LNP and LFNP were tested by the DPPH method and their RSAs were calculated using Eq. (1), as shown in Fig. 8. The RSA of LNP was 80.8%, and the antioxidant activity of LFNP became stronger with the increase of citric acid addition, and the RSA of LFNP-3 reached 96.7%.

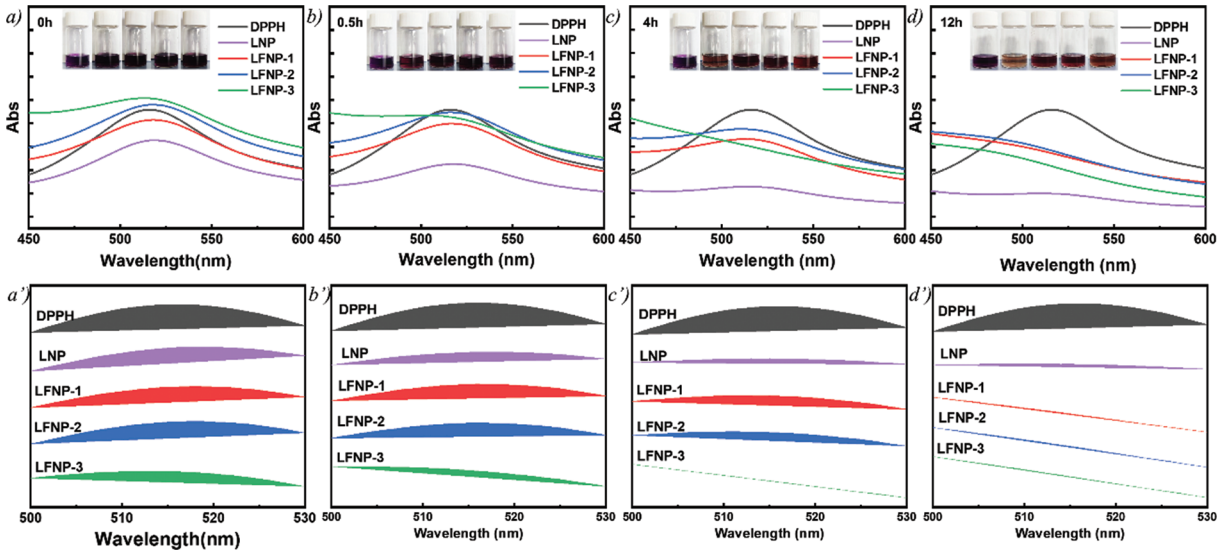

Figure 8: Antioxidant properties of lignin treated with different qualities of citric acid (a, a') 0 h; (b, b') 0.5 h; (c, c') 4 h; and (d, d') 12 h

Fig. 8 shows the corresponding image where the color of the DPPH solution changes from purple to light purple or yellow. The RSA values at different moments were listed in Table 2, and it can be found that the free radical scavenging ability of LFNP-1 and LFNP-2 at 4 h was lower than that of LNP, but the RSA value of LFNP-3 reached 96.5%, which was already better than that of LNP (69.2%). The lower RSA values of LFNP-1 and LFNP-2 at 0h and 4 h compared to LNP may be related to the dispersion of particles in the solvent and the degree of group exposure. It can be seen that the RSA values of LFNP were higher than those of LNP at 12 h, which was enough to prove that the antioxidant ability of LFNP was higher than

that of LNP. The antioxidant mechanism of lignin mainly depends on the capture of reactive radicals by phenoxy radicals and H· by lignin [62,63]. Therefore, the main reason for the enhanced antioxidant activity of modified lignin is that nitrogen-containing groups as electron donors are more likely to form stable phenoxyl radicals and reduce the enthalpy of cleavage of phenolic hydroxyl groups, which in turn makes it easier to form stable phenoxyl radicals and H· in the phenolic structure of LNP [64]. In modified lignin molecules, the behavior of lone pairs of marginal nitrogen atoms, electron transfer, and other behaviors that cause electron cloud arrangements all lead to enhanced antioxidant activity.

Table 2: RSA rate with different time of LFNP-1, LFNP-2 and LFNP-3 samples

Samples	LNP (%)	LFNP-1 (%)	LFNP-2 (%)	LFNP-3 (%)
0.5	36.8	8.2	16.3	59.0
4.0	69.2	37.7	48.9	96.5
12.0	80.8	93.1	94.7	96.7

4 Conclusions

In summary, we proposed a one-step hydrothermal reaction method for the rapid synthesis of LFNP using LNP in the presence of CA and EDA, and the newly synthesized LFNP had good dispersion in water. The LFNP were mainly composed of aromatic ring structures containing amide groups, and they exhibited excitation-related fluorescence behaviors under excitation of 375–385 nm, with the maximum emission wavelengths in the range of 454–465 nm, and it was found that the fluorescence intensity increased with the increase of CA addition. With the gradual increase of excitation wavelength, the maximum fluorescence emission of LFNP remained essentially constant, reflecting the fluorescence stability. The antioxidant activity assay was performed using the DPPH radical scavenging method and the RSA value of LFNP-3 was found to be 96.7%. This study provides a new strategy for the preparation of multifunctional nanoparticles with fluorescence and high bioactivity, and offers a new idea for expanding their applications in biomedical fields.

Acknowledgement: This manuscript is grateful for the strong support from the National Natural Science Foundation of China (51903106), State Administration of Foreign Experts Affairs (G2021144006L). Thanks to the School of Chemistry and Materials Engineering at Jiangnan University. We also thank everyone who provided feedback and suggestions during the experiment and writing process.

Funding Statement: This work was financially supported by National Natural Science Foundation of China (51903106), State Administration of Foreign Experts Affairs (G2021144006L).

Author Contributions: The authors confirm contribution to the paper as follows: Xujing Zhang, Hatem Abushammala, Debora Puglia, Binbao Lu, Pengwu Xu, Weijun Yang, Piming Ma: data curation, writing-original draft, methodology, formal analysis. Weijun Yang: writing-revising draft, funding support, conceptualization and validation. All authors reviewed the results and approved the final version of the manuscript.

Availability of Data and Materials: The authors are unable or have chosen not to specify which data has been used.

Conflicts of Interest: The authors declare that they have no conflicts of interest to report regarding the present study.

References

1. Phongpreecha T, Hool NC, Stoklosa RJ, Klett AS, Foster CE, Bhalla A, et al. Predicting lignin depolymerization yields from quantifiable properties using fractionated biorefinery lignins. Green Chem. 2017;19(21):5131–43. doi:10.1039/c7gc02023f.
2. Gómez-Monedero B, Ruiz MP, Bimbela F, Faria J. Selective hydrogenolysis of α-O-4, β-O-4, 4-O-5 C-O bonds of lignin-model compounds and lignin-containing stillage derived from cellulosic bioethanol processing. Appl Catal A: Gen. 2017;541:60–76. doi:10.1016/j.apcata.2017.04.022.
3. Zhu LL, Zhong ZP. Effects of cellulose, hemicellulose and lignin on biomass pyrolysis kinetics. Korean J Chem Eng. 2020;37(10):1660–8. doi:10.1007/s11814-020-0553-y.
4. Yue FX, Lu FC, Ralph S, Ralph J. Identification of 4-O-5-units in softwood lignins via definitive lignin models and NMR. Biomacromolecules. 2016;17(6):1909–20. doi:10.1021/acs.biomac.6b00256.
5. Karlsson M, Romson J, Elder T, Emmer A, Lawoko M. Lignin structure and reactivity in the organosolv process studied by NMR spectroscopy, mass spectrometry, and density functional theory. Biomacromolecules. 2023;24(5):2314–26. doi:10.1021/acs.biomac.3c00186.
6. Ragauskas AJ, Beckham GT, Biddy MJ, Chandra R, Chen F, Davis MF, et al. Lignin valorization: improving lignin processing in the biorefinery. Science. 2014;344(6185):709. doi:10.1126/science.1246843.
7. Upton BM, Kasko AM. Strategies for the conversion of lignin to high-value polymeric materials: review and perspective. Chem Rev. 2016;116(4):2275–306. doi:10.1021/acs.chemrev.5b00345.
8. Zhou P, Xu J, Hou X, Dai L, Zhang J, Xiao X, et al. Heteroatom-engineered multicolor lignin carbon dots enabling bimodal fluorescent off-on detection of metal-ions and glutathione. Int J Biol Macromol. 2023;253:126714. doi:10.1016/j.ijbiomac.2023.126714.
9. Kwon W, Lee G, Do S, Joo T, Rhee SW. Size-controlled soft-template synthesis of carbon nanodots toward versatile photoactive materials. Small. 2014;10(3):506–13. doi:10.1002/small.201301770.
10. Zhu SJ, Meng QN, Wang L, Zhang JH, Song YB, Jin H, et al. Highly photoluminescent carbon dots for multicolor patterning, sensors, and bioimaging. Angew Chem Int Ed. 2013;52(14):3953–57. doi:10.1002/anie.201300519.
11. Baker SN, Baker GA. Luminescent carbon nanodots: emergent nanolights. Angew Chem Int Ed. 2010;49(38):6726–44. doi:10.1002/anie.200906623.
12. Wang YR, Zhang L, Wu YL, Zhong YJ, Hu Y, Lou XW. Carbon-coated Fe_3O_4 microspheres with a porous multideck-cage structure for highly reversible lithium storage. Chem Commun. 2015;51(32):6921–4. doi:10.1039/c5cc01251a.
13. Zhu SJ, Song YB, Zhao XH, Shao JR, Zhang JH, Yang B. The photoluminescence mechanism in carbon dots (graphene quantum dots, carbon nanodots, and polymer dots): current state and future perspective. Nano Res. 2015;8(2):355–81. doi:10.1007/s12274-014-0644-3.
14. Guo X, Wang CF, Yu ZY, Chen L, Chen S. Facile access to versatile fluorescent carbon dots toward light-emitting diodes. Chem Commun. 2012;48(21):2692–4. doi:10.1039/c2cc17769b.
15. Yang YH, Cui JH, Zheng MT, Hu CF, Tan SZ, Xiao Y, et al. One-step synthesis of amino-functionalized fluorescent carbon nanoparticles by hydrothermal carbonization of chitosan. Chem Commun. 2012;48(3):380–82. doi:10.1039/c1cc15678k.
16. Liu SS, Wang CF, Li CX, Wang J, Mao LH, Chen S. Hair-derived carbon dots toward versatile multidimensional fluorescent materials. J Mater Chem. 2014;2(32):6477–83. doi:10.1039/c4tc00636d.
17. Sahu S, Behera B, Maiti TK, Mohapatra S. Simple one-step synthesis of highly luminescent carbon dots from orange juice: application as excellent bio-imaging agents. Chem Commun. 2012;48(70):8835–7. doi:10.1039/C2CC33796G.
18. Si MY, Zhang J, He YY, Yang ZQ, Yan X, Liu MR, et al. Synchronous and rapid preparation of lignin nanoparticles and carbon quantum dots from natural lignocellulose. Green Chem. 2018;20(15):3414–9. doi:10.1039/c8gc00744f.
19. El-Shabasy RM, Elsadek MF, Ahmed BM, Farahat MF, Mosleh KN, Taher MM. Recent developments in carbon quantum dots: properties, fabrication techniques, and bio-applications. Processes. 2021;9(2):388. doi:10.3390/pr9020388.

20. Yang W, Ding H, Puglia D, Kenny J, Liu T, Guo J, et al. Bio-renewable polymers based on lignin-derived phenol monomers: synthesis, applications, and perspectives. SusMat. 2022;2:535–68. doi:10.1002/sus2.87.
21. Peng Z, Jiang X, Si C, Cárdenas Oscanoa A, Huang C. Advances of modified lignin as substitute to develop lignin-based phenol-formaldehyde resin adhesives. ChemSusChem. 2023;16:e202300174. doi:10.1002/cssc.202300174.
22. Culebras M, Beaucamp A, Wang Y, Clauss MM, Frank E, Collins MN. Biobased structurally compatible polymer blends based on lignin and thermoplastic elastomer polyurethane as carbon fiber precursors. ACS Sustain Chem Eng. 2018;6(7):8816–25. doi:10.1021/acssuschemeng.8b01170.
23. Xue BL, Wen JL, Sun RC. Lignin-based rigid polyurethane foam reinforced with pulp fiber: synthesis and characterization. ACS Sustain Chem Eng. 2014;2(6):1474–80. doi:10.1021/sc5001226.
24. Zhang D, Zeng J, Liu W, Qiu X, Qian Y, Zhang H, et al. Pristine lignin as a flame retardant in flexible PU foam. Green Chem. 2021;23:5972–80. doi:10.1039/D1GC01109J.
25. Culebras M, Sanchis MJ, Beaucamp A, Carsí M, Kandola BK, Horrocks AR, et al. Understanding the thermal and dielectric response of organosolv and modified kraft lignin as a carbon fibre precursor. Green Chem. 2018;20(19): 4461–72. doi:10.1039/c8gc01577e.
26. Han Y, Wang Y, Zhao B, Bai Y, Han S, Yahui Z, et al. Carbon dots: building a robust optical shield for wood preservation. Adv Compos Hybrid Mater. 2023;6:39. doi:10.1007/s42114-022-00619-8.
27. Chen WX, Hu CF, Yang YH, Cui JH, Liu YL. Rapid synthesis of carbon dots by hydrothermal treatment of lignin. Materials. 2016;9(3):184. doi:10.3390/ma9030184.
28. Ding ZY, Li FF, Wen JL, Wang XL, Sun RC. Gram-scale synthesis of single-crystalline graphene quantum dots derived from lignin biomass. Green Chem. 2018;20(6):1383–90. doi:10.1039/c7gc03218h.
29. Liang ZC, Zeng L, Cao XD, Wang Q, Wang XH, Sun RC. Sustainable carbon quantum dots from forestry and agricultural biomass with amplified photoluminescence by simple NH4OH passivation. J Mater Chem. 2014;2(45):9760–6. doi:10.1039/c4tc01714e.
30. Xie YD, Cheng DD, Liu XL, Han AX. Green hydrothermal synthesis of n-doped carbon dots from biomass highland barley for the detection of Hg^{2+}. Sensors. 2019;19(14):3169. doi:10.3390/s19143169.
31. Pang ZZ, Fu YJ, Yu HL, Liu SW, Yu ST, Liu YX, et al. Efficient ethanol solvothermal synthesis of high-performance nitrogen-doped carbon quantum dots from lignin for metal ion nanosensing and cell imaging. Ind Crops Prod. 2022;183:114957. doi:10.1016/j.indcrop.2022.114957.
32. Zhang Z, Terrasson V, Guénin E. Lignin nanoparticles and their nanocomposites. Nanomaterials. 2021;11(5):1336. doi:10.3390/nano11051336.
33. Wen JL, Sun SL, Xue BL, Sun RC. Recent advances in characterization of lignin polymer by solution-state nuclear magnetic resonance (NMR) methodology. Materials. 2013;6(1):359–91. doi:10.3390/ma6010359.
34. Yang W, Owczarek JS, Fortunati E, Kozanecki M, Mazzaglia A, Balestra GM, et al. Antioxidant and antibacterial lignin nanoparticles in polyvinyl alcohol/chitosan films for active packaging. Ind Crops Prod. 2016;94:800–11. doi:10.1016/j.indcrop.2016.09.061.
35. Shen Q, Xue YY, Zhang Y, Li TJ, Yang TW, Li SR. Effect of microstructure-scale features on lignin fluorescence for preparation of high fluorescence efficiency lignin-based nanomaterials. Int J Biol Macromol. 2022;202:520–8. doi:10.1016/j.ijbiomac.2022.01.095.
36. Zhang MN, Long X, Ma YS, Wu SG. Re-discussion on the essence of the ultra-bright fluorescent carbon dots synthesized by citric acid and ethylenediamine. Optical Mat. 2022;135:113311. doi:10.1016/j.optmat.2022. 113311.
37. Yang XX, Hou SY, Chu TT, Han JZ, Li RS, Guo YZ, et al. Preparation of magnesium, nitrogen-codoped carbon quantum dots from lignin with bright green fluorescence and sensitive pH response. Ind Crops Prod. 2021;167: 113507. doi:10.1016/j.indcrop.2021.113507.
38. Jing SS, Zhao YS, Sun RC, Zhong LX, Peng XW. Facile and high-yield synthesis of carbon quantum dots from biomass-derived carbons at mild condition. ACS Sustain Chem Eng. 2019;7(8):7833–43. doi:10.1021/ acssuschemeng.9b00027.

39. Wang G, Guo GL, Chen D, Liu ZD, Zheng XH, Xu AL, et al. Facile and highly effective synthesis of controllable lattice sulfur-doped graphene quantum dots via hydrothermal treatment of durian. ACS Appl Mater Interfaces. 2018;10(6):5750–9. doi:10.1021/acsami.7b16002.
40. Bulota M, Tanpichai S, Hughes M, Eichhorn SJ. Micromechanics of TEMPO-oxidized fibrillated cellulose composites. ACS Appl Mater Interfaces. 2012;4(1):331–7. doi:10.1021/am201399q.
41. Xue BL, Yang Y, Sun YC, Fan JS, Li XP, Zhang Z. Photoluminescent lignin hybridized carbon quantum dots composites for bioimaging applications. Int J Biol Macromol. 2019;122:954–61. doi:10.1016/j.ijbiomac.2018.11.018.
42. Xue YY, Qiu XQ, Ouyang XP. Insights into the effect of aggregation on lignin fluorescence and its application for microstructure analysis. Int J Biol Macromol. 2020;154:981–8. doi:10.1016/j.ijbiomac.2020.03.056.
43. Cao MY, Zhao XJ, Gong X. Ionic liquid-assisted fast synthesis of carbon dots with strong fluorescence and their tunable multicolor emission. Small. 2022;18(11):2106683. doi:10.1002/smll.202106683.
44. Liang JX, Pan ZH, Zhang K, Yang DZ, Tai JW, Wang CK, et al. A facile method to achieve red thermally activated delayed fluorescence emitters with EQE over 30% via molecular aspect ratio engineering. Chem Eng J. 2023;457:141074. doi:10.1016/j.cej.2022.141074.
45. Zu HY, Fan CC, Liu CD, Jing CQ, Chai CY, Liang BD, et al. Establishing a relationship between the bandgap and the structure in 2D lead halide perovskite semiconductors. Chem Mater. 2023;35(15):5854–63. doi:10.1021/acs.chemmater.3c00596.
46. Liu YS, Yang HY, Wang Y, Ma CH, Luo S, Wu ZW, et al. Fluorescent thermochromic wood-based composite phase change materials based on aggregation-induced emission carbon dots for visual solar-thermal energy conversion and storage. Chem Eng J. 2021;424:130426. doi:10.1016/j.cej.2021.130426.
47. Polyakov IV, Grigorenko BL, Epifanovsky EM, Krylov AI, Nemukhin AV. Potential energy landscape of the electronic states of the GFP chromophore in different protonation forms: electronic transition energies and conical intersections. J Chem Theory Comput. 2010;6(8):2377–87. doi:10.1021/ct100227k.
48. Wang Z, Cao LJ, Ding YM, Shi R, Wang XJ, Lu H, et al. One-step and green synthesis of nitrogen-doped carbon quantum dots for multifunctional electronics. RSC Adv. 2017;7(35):21969–73. doi:10.1039/c7ra03840b.
49. Kumar GS, Roy R, Sen D, Ghorai UK, Thapa R, Mazumder N, et al. Amino-functionalized graphene quantum dots: origin of tunable heterogeneous photoluminescence. Nanoscale. 2014;6(6):3384–91. doi:10.1039/c3nr05376h.
50. Wang RY, Fan HL, Jiang W, Ni GS, Qu SJ. Amino-functionalized graphene quantum dots prepared using high-softening point asphalt and their application in Fe^{3+} detection. Appl Surf Sci. 2019;467:446–55. doi:10.1016/j.apsusc.2018.10.104.
51. Peng ZX, Zhang K, Huang ZW, Wang ZB, Duttwyler S, Wang YG, et al. Emissions from a triphenylamine-benzothiadiazole-monocarbaborane triad and its applications as a fluorescent chemosensor and a white OLED component. J Mater Chem. 2019;7(8):2430–5. doi:10.1039/c8tc06176a.
52. Orita R, Franckevicius M, Vysniauskas A, Gulbinas V, Sugiyama H, Uekusa H, et al. Enhanced fluorescence of phthalimide compounds induced by the incorporation of electron-donating alicyclic amino groups. Phys Chem Chem Phys. 2018;20(23):16033–44. doi:10.1039/c8cp01999a.
53. Lu H, Feng LL, Li SS, Zhang J, Lu HF, Feng SY. Unexpected strong blue photoluminescence produced from the aggregation of unconventional chromophores in novel siloxane-poly(amidoamine) dendrimers. Macromolecules. 2015;48(3):476–82. doi:10.1021/ma502352x.
54. Li Y, Shen Q, Li SR, Xue YY. High quantum-yield lignin fluorescence materials based on polymer confinement strategy and its application as a natural ratiometric pH sensor film. Ind Crops Prod. 2023;194:116384. doi:10.1016/j.indcrop.2023.116384.
55. Wu JQ, Li T, Qiu XQ, Qin YL, Chen LH. γ-Valerolactone/H_2O binary solvent for one-pot preparation and functional tailoring of lignin-based carbon dots. ACS Sustain Chem Eng. 2023;11(33):12256–64. doi:10.1021/acssuschemeng.3c01411.

56. Takada M, Okazaki Y, Kawamoto H, Sagawa T. Tunable light emission from lignin: various photoluminescence properties controlled by the lignocellulosic species, extraction method, solvent, and polymer. ACS Omega. 2022;7(6):5096–103. doi:10.1021/acsomega.1c06104.
57. He XY, Luzi F, Yang WJ, Xiao ZF, Torre L, Xie YJ, et al. Citric acid as green modifier for tuned hydrophilicity of surface modified cellulose and lignin nanoparticles. ACS Sustain Chem Eng. 2018;6(8):9966–78. doi:10.1021/acssuschemeng.8b01202.
58. Qin L, Li WC, Zhu JQ, Liang JN, Li BZ, Yuan YJ. Ethylenediamine pretreatment changes cellulose allomorph and lignin structure of lignocellulose at ambient pressure. Biotechnol Biofuels. 2015;8:174. doi:10.1186/s13068-015-0359-z.
59. Song SS, Su D, Xu XX, Yang XY, Wei LG, Li KL, et al. Using citric acid to suppress lignin repolymerization in the organosolv pretreatment of corn stalk. Ind Crops Prod. 2023;200:116881. doi:10.1016/j.indcrop.2023.116881.
60. Xu L, Zhang JY, Zong QJ, Wang L, Xu T, Gong JB, et al. High-solid ethylenediamine pretreatment to fractionate new lignin streams from lignocellulosic biomass. Chem Eng J. 2021;427:130962. doi:10.1016/j.cej.2021.130962.
61. Shi T, Xu L, Wang YN, Liu SC, Liu ZH, Zhao GJ, et al. Aminated and amidated structures introduced by ethylenediamine pretreatment endow lignin with bright fluorescence. Green Chem. 2022;24(23):9040–54. doi:10.1039/d2gc02120j.
62. Yang WJ, Fortunati E, Gao DQ, Balestra GM, Giovanale G, He XY, et al. Valorization of acid isolated high yield lignin nanoparticles as innovative antioxidant/antimicrobial organic materials. ACS Sustain Chem Eng. 2018;6(3):3502–14. doi:10.1021/acssuschemeng.7b03782.
63. Yang WJ, Ding H, Qi GC, Guo JQ, Xu F, Li CC, et al. Enhancing the radical scavenging activity and UV resistance of lignin nanoparticles via surface mannich amination toward a biobased antioxidant. Biomacromolecules. 2021;22(6):2693–701. doi:10.1021/acs.biomac.1c00387.
64. Kattamuri PV, Yin J, Siriwongsup S, Kwon DH, Ess DH, Li Q, et al. Practical singly and doubly electrophilic aminating agents: a new, more sustainable platform for carbon-nitrogen bond formation. J Am Chem Soc. 2017;139(32):11184–96. doi:10.1021/jacs.7b05279.